

Effective Super-Resolution Method for Paired Electron Microscopic Images

Yanjun Qian, Jiayi Xu, Lawrence F. Drummy, and Yu Ding, *Senior Member, IEEE*

Abstract—This paper is concerned with developing super-resolution algorithms for handling electron microscopic images. We note two main aspects differentiating the problem discussed here from existing approaches in the super-resolution literature. The first difference is that in the electron imaging setting, we have a pair of physical high-resolution and low-resolution images, rather than a physical image with its downsampled counterpart. The high-resolution image covers about 25% of the view field of the low-resolution image, and the objective is to enhance the area of the low-resolution image where there is no high-resolution counterpart. The second difference is that the physics behind electron imaging is different from that of optical (visible light) photos. The implication is that super-resolution methods trained by optical photos are not going to be effective when applied to electron images. Focusing on the unique properties, we propose a new super-resolution image algorithm entailing the following components: (a) a global and local registration method to match the high- and low-resolution image patches; (b) a clustering method that selects the representative patches for a paired library, and (c) a non-local-mean method that reconstructs the high-resolution image using the paired library. Tested on 22 pairs of electron microscopic images, we find that the proposed method outperforms considerably the existing super-resolution methods. A noteworthy merit of the proposed method lies in its superior ability to suppress background noise without deteriorating the quality of the foreground signal.

Index Terms—Electron microscopic image, global and local registration, library-based non-local mean filter, paired-image super-resolution.

I. INTRODUCTION

In this paper, we consider an image processing problem encountered in nanomaterial characterization. Material science researchers capture a pair of multi-resolution electron microscopic (EM) images: a high-resolution (HR) image of $M \times N$ pixels, denoted by I_h , and a low-resolution (LR) image, denoted by I_l , with the same amount of pixels but half of the resolution of I_h . As a result, the HR image covers only 25% of the area that is covered by the LR image. Figure 1 demonstrates two pairs of such EM images, both obtained by a scanning electron microscope (SEM). The overlapping areas in the LR images are marked by the red rectangles. The objective is to develop a super-resolution (SR) method for reconstructing an HR image of $2M \times 2N$ pixels over the whole area that is covered by the LR image (which is our

field-of-view). The essence of the task is to enhance the area of the low-resolution image where there is no high-resolution counterpart. If a method can accomplish this research goal, material scientists can effectively survey a bigger area with imaging quality comparable to HR images but with less dense sampling.

HR images are desired for the purpose of material characterization because they capture and reveal fine structures of nanomaterials [1, 2, 3, 4], but it is time consuming to capture HR images. While using a SEM or transmission electron microscope (TEM), the images are created by an electron beam rastering through the material, so that the time cost will be at least proportional to the number of pixels. An equally important consideration is that the electron beam of an EM may damage the subtle structure of certain materials. Material science experts want to avoid dense sampling in electron imaging if at all possible. An effective SR approach, if available, can be of a great help to high resolution electron imaging of materials.

In recent years, numerous SR works have been proposed and reported [5, 6, 7, 8]. We note two important differences, distinguishing the problem at hand from those considered in the existing SR literature. The first difference is that we have a pair of LR and HR images, both physical and obtained independently, rather than a physical HR image with its downsampled version. It is our understanding that the vast majority of the existing SR approaches take the downsampled version of the HR images as their LR image inputs. We find that having the LR physical images presents unique challenges that the existing SR approaches are ill-equipped to handle. We will present a preliminary analysis with quantitative evidence in Section II.

The second difference is that the physics behind electron imaging is different from that of optical photos taken under visible light. The implication is that super-resolution methods trained by optical photos are not going to be effective when applied to electron images. But available EM images are much fewer than the amount of publicly available optical images, and they also vary a lot with different EM parameter settings and various types of nanomaterials. Using the relatively small number of EM images at hand does not produce a competent SR method out of the existing framework. Again, we will provide quantitative evidence in Section II to support our claim.

Focusing on the unique properties of our problem, we propose an SR framework comprising the following steps. First, we devise a global and local registration algorithm to identify the overlapping area and handle the local distortions

Y. Qian is with the Department of Statistical Sciences and Operations Research, Virginia Commonwealth University, Richmond, Virginia 23220 USA. E-mail: yqian3@vcu.edu.

J. Xu and Y. Ding are with the Department of Industrial & Systems Engineering, Texas A&M University, College Station, Texas 77843 USA.

L. Drummy is with the Materials and Manufacturing Directorate, Air Force Research Laboratory, Wright-Patterson Air Force Base, OH 45433 USA.

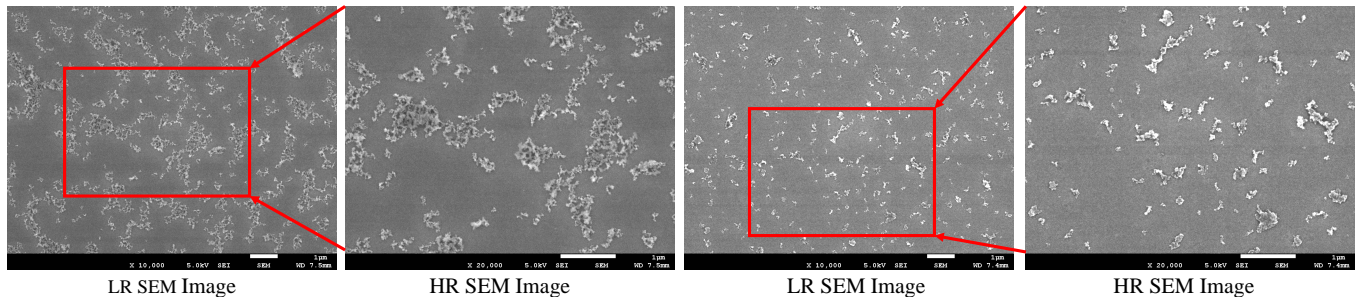


Fig. 1. Two pairs of LR and HR SEM images. The red rectangles in the LR images are the areas corresponding to the HR images.

between the two paired images. Then we build a paired library to connect the HR and LR patches from the training images. To include the informative patches for better training results, we design a clustering method for selecting the representative patches. The last step is a revised library-based non-local-mean (LB-NLM) method that reconstructs the HR images over the whole field of view, using the paired library of representative patches. Using 22 pairs of EM images, we demonstrate that the proposed SR method do render considerable benefit over the existing SR approaches.

The remaining parts of this paper are organized as follows. Section II reviews the relevant literature and presents our preliminary analysis, which is to demonstrate what happens when the existing SR methods are applied to our problem. Section III introduces the main components in the proposed SR framework for paired EM images. Section IV compares the proposed method with the existing SR approaches. In Section V, we summarize our contributions and discuss possible extensions.

II. LITERATURE REVIEW AND PRELIMINARY ANALYSIS

The early SR literature focuses on restoring an HR image with multiple LR images (e.g., those in a short clip of video) by recovering the lost information from subpixel shifts [5, 9, 10]. However, these methods hardly work on static images. Since Freeman et al. [11] proposed the single-image SR algorithm, the learning-based methods have become the mainstream in the SR research field. HR/LR patches are extracted from a set of training images, and a machine learning model is then built to map the images at the two resolutions. A testing LR image will be segmented into overlapping patches, and the corresponding HR patches are to be inferred by the trained model. The HR image over the whole field of view is then reconstructed from these HR patches.

Numerous single-image SR methods for optical images have been proposed using different machine learning models. The neighborhood embedding (NE) algorithms [12, 13, 14] are based on the assumption that the HR and LR patches share similar manifold structures. An HR patch is estimated from the nearest neighbors of its LR counterpart in the manifold. The joint model methods [15, 16] learn a joint HR-LR patch distribution and predict HR images by maximizing the likelihood. The regression-based algorithms [17, 18, 19, 20] fit a regression model to map LR and HR patches and predict the

HR patch using the LR patches as the regressors. The coding-based methods [21, 22, 23] look for a parsimonious dictionary to encode the patches and reconstruct the HR patch from the coefficients of its LR counterpart. In recent years, the deep learning methods [24, 25, 26] have been adopted for the single-image SR, which train deep neural networks, from training samples, with the LR patches as the inputs and HR ones as the outputs. The deep learning methods can be considered as generalized regression methods with complicated nonlinear mapping structures.

For optical images, the deep learning based SR methods achieve the best performance in terms of the reconstruction accuracy, measured by both peak signal-to-noise ratio (PSNR) and structural similarity (SSIM) [27]. In a recent single-image challenge, NTIRE 2017 [8], almost all the competitive algorithms adopt the deep learning approach. That is why the deep learning based SR methods become our first choice when we attempt to solve the SR problem for paired EM images. Specifically, we implement the very-deep super-resolution method (VDSR) [25], as the authors of VDSR provide detailed guidance for implementation and VDSR's performance is very close to the best one in NTIRE 2017.

In its default setting, VDSR trains neural networks from hundreds of HR optical images and their downsampled versions serving as the LR images. The same method (VDSR) can be applied to the HR electron images and their downsampled counterparts and train a deep neural network for EM images. That is what we did. First, we choose 539 HR optical images from the IAPR TC-12 Benchmark [28] and sample 256 patches from each image. We train a neural network with 41 layers on these patches with the scale factor 2.0. Other parameters, such as the training rate and the maximum number of iterations, are set as the default values in [25]. Second, we collect 539 HR nanoimages captured by EMs and again sample 256 patches per image. With the same neural network structure and parameter setting, we train another VDSR model using the EM data. We denote the VDSR trained on optical images by *Net_Optical*, and the VDSR trained on electron images by *Net_EM*.

For testing, we prepare two datasets: synthetic electron images downsampled from the HR images and the physical LR electron images corresponding to the same HR images. Either image option is used as the input for enhancement via the resulting VDSR. After that, we compare the reconstructed

images, presumably enhanced, with the actual HR images and calculate the PSNR—a high PSNR indicates a good reconstruction. Our baseline method is the bicubic interpolation [29], which is the most popular algorithm for upsampling an LR image to the pixel amount of the HR images. For the baseline method, we upsample our LR EM image using bicubic interpolation by a factor of two and calculate the PSNR of the resulting interpolated images. A competitive SR method is supposed to produce a higher PSNR than bicubic interpolation.

Figure 2 presents the change in PSNR when the two versions of VDSR are applied to the two test datasets, in relative to the PSNR resulting from applying the bicubic interpolation baseline method to the same images. A value of zero in Figure 2 means that VDSR returns the same PSNR as bicubic interpolation, a positive value means actual improvement over bicubic interpolation, and a negative value means a performance deterioration as compared with bicubic interpolation.

In Figure 2, left panel, when applying to the downsampled images, both versions of VDSR improve upon bicubic interpolation, but the improvement made by *Net_EM* is appreciably greater than that made by *Net_Optical*. This provides one example supporting our conjecture that VDSR trained by optical images are less effective than that trained by electron images. In Figure 2, right panel, when applying to the physical LR electron images, both versions of VDSR perform worse relative to bicubic interpolation. Again the *Net_Optical* version is worse than the *Net_EM* version, although the difference between the two versions in this case is less pronounced than when both versions of VDSR are applied to the downsampled images.

Our observation based on the above example suggests that while both problems identified above, i.e., the paired physical images and the electron-versus-optical images, cause the existing SR approaches ineffective in addressing our research challenge, the paired physical image problem appear to be the major one.

In the existing SR methods, the synthetic LR images are created by blurring HR images with a Gaussian kernel and then downsampling the blurred images. This approach is not suitable when physical LR images are used because the properties of physical LR images do not necessarily satisfy the downsampling model. In Figure 3, we compare a physical

LR electron image and a synthetic image, downsampled from their commonly paired HR image, and demonstrate their discrepancy. As we see in the right most plot of Figure 3, the difference between the two images is rather pronounced. We believe that the reason of discrepancy is in fact complicated, caused by the noise existing in the HR image, the different contrast levels between the paired images, and/or different natures and degrees of local distortion from individual image-capturing processes.

Sreehari *et al.* [30] propose one of the first SR methods for EM images. In their approach, a library is built by an HR scan over a small field-of-view of a certain sample. When the LR EM image over a large field-of-view comes, a library-based non-local-mean method (LB-NLM) is applied to the upsampled image. After that, the HR image is recovered in a plug-and-play framework by invoking an alternating direction method of multipliers (ADMM) solver [31]. Compared with the SR methods for optical images, Sreehari *et al.* [30] build the library using image samples of nanomaterials, rather than unrelated optical images, and consider the noise in HR images explicitly in the plug-and-play framework. However, their algorithm does not include the physical LR electron images in the library, falling short of mapping the LR and HR patches directly. Moreover, it only handles the noise in HR images without considering local distortions and different contrasts between the multi-resolution image data.

Although not studied in the SR literature as thoroughly as the single-image SR problems have been, there are in fact some initial attempts on the paired images SR problem. In a very recent publication, Zhang *et al.* [32] discuss the SR issue when a physical LR image is involved, but their work is still for optical images. They improve the traditional deep learning based SR from the following two aspects. The first action is that they use the raw data captured by a camera sensor, rather than the processed RGB images, as the raw data contains more information. The second action is to introduce a new loss function for handling the local distortions between the captured LR and HR images. Their method outperforms SR approaches that use synthetic images for training.

For the first aspect of improvement advocated by Zhang *et al.* [32], i.e., using the raw images from a camera devices, it is complicated to do so when electron microscopes are involved. So in this paper, we stay with the processed images produced by an EM’s camera device and the associated operating system. We do resonant with the second aspect of improvement advocated by Zhang *et al.* [32], i.e., addressing the local distortion problem. We in fact independently identified this problem before seeing Zhang *et al.* [32] but we devised a different approach. Our approach borrows certain ideas from Sreehari *et al.* [30] and adds new components to make it more effective on the paired EM images.

III. SUPER-RESOLUTION METHOD FOR PAIRED EM IMAGES

The proposed method consists of three components: (a) a global and local registration method to match patches between LR/HR images, (b) a clustering algorithm to select the representative pairs into a paired library, and (c) a revised LB-NLM

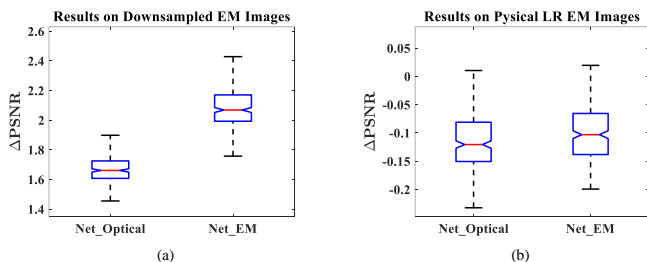


Fig. 2. The performance of VDSR when its two versions, *Net_Optical* and *Net_EM*, are applied to the downsampled and physical LR EM images, respectively.

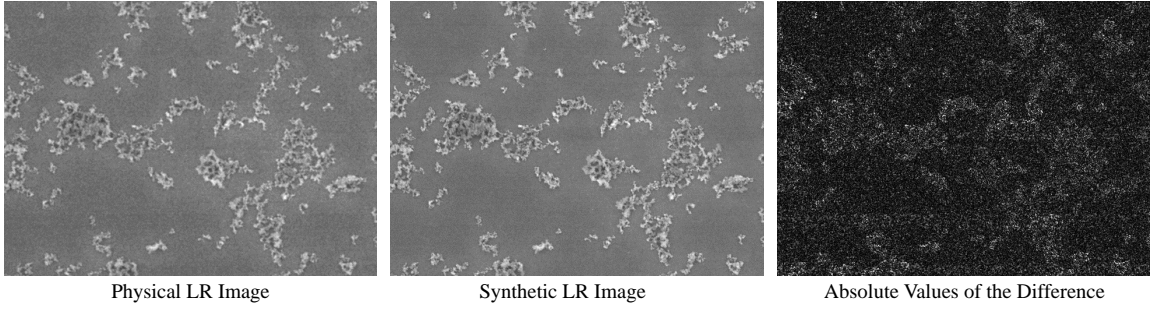


Fig. 3. Comparison of a physical LR EM image and the synthetic downsampled image from the common corresponding HR image.

filter to reconstruct an HR image using the paired library. The idea and procedure of each component is described in the subsequent subsections. In the last subsection, Section III-D, we discuss the performance criteria used to evaluate the efficacy of the proposed method. Those include PSNR and SSIM mentioned above. We also introduce some new metrics that we believe can articulate more pointedly the improvement made by the proposed method.

A. Global & Local Registration

With a pair of HR/LR EM images, \mathbf{I}_h and \mathbf{I}_l , as inputs, we upsample \mathbf{I}_l by two times using the bicubic interpolation; this produces \mathbf{I}_u . Then a shift transform (x, y) and a rotation transform (θ) are estimated by comparing the overlapping area of \mathbf{I}_h and \mathbf{I}_u . To accelerate the matching process, we first downsample the two images and estimate (x, y, θ) with a grid search, and then refine the estimation using the original images. The registered upsampled image is denoted by \mathbf{I}_r .

For the local registration, we segment the matched \mathbf{I}_h and \mathbf{I}_r into $n \times n$ overlapping patches. $\mathbf{P}_h(i, j)$ and $\mathbf{P}_r(i, j)$ denote the patches centered at (i, j) in \mathbf{I}_h and \mathbf{I}_r . Then we search the neighborhood of (i, j) to find (i^*, j^*) via solving the following optimization problem:

$$\min_{i^*, j^*} \frac{\mathbf{P}_h(i^*, j^*) \cdot \mathbf{P}_r(i, j)}{\|\mathbf{P}_h(i^*, j^*)\|_2 \|\mathbf{P}_r(i, j)\|_2}, \quad (1)$$

where \cdot denotes the inner product and $\|\cdot\|_2$ is the l_2 normal of the patch. We prefer the use of an inner product to Euclidean distance to match the two patches as the former is insensitive to the contrast difference between the two images. This criterion become less effective when the patches contain poor texture. Fortunately, the patches containing poor texture are the background patches, which are less important to the mission of super-resolution. We only apply the local registration to the patches with rich texture, which can be selected by deeming the variance of $\mathbf{P}_r(i, j)$ of a patch larger than a certain threshold. For our EM images, we set the threshold as 100. Figure 4 presents one examples after local registration, where the red arrows illustrate the displacements $(i^* - i, j^* - j)$ between the matched patches in \mathbf{I}_h and \mathbf{I}_r . The magnitudes and directions of the displacements vary significantly across the image, showing a complex and irregular pattern of local distortions, which would not have been adjusted by a global registration alone.

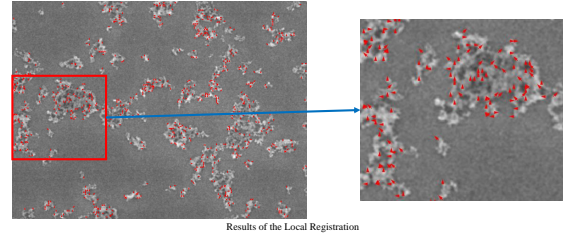


Fig. 4. The results of the local registration. The right figure is magnified from the red rectangle in the left figure, in which the red arrows indicate the displacements $(i^* - i, j^* - j)$ between the matched patches.

B. Representative Paired-Library Building

After the local registration, we store the matched patches from \mathbf{P}_h 's and \mathbf{P}_r 's into a paired library. Including \mathbf{P}_r 's, the upsampled physical LR images, into the library is a key difference between the proposed method and the original LB-NLM method [30], which uses the HR patches only.

Sreehari et al. [30] propose to create a library with dense sampling. We find that approach can be improved. The training area of each pair of EM images has about one million overlapping patches and many of them are of low texture and redundant information. We could, and should, reduce the library size to improve the learning efficiency. As a large portion of the patches belongs to the background, random sampling is understandably not the most effective approach for patch selection. To ensure that different categories of image patches are adequately included, such as foreground, background, and boundaries, we devise a k -means clustering method to build the paired library, which is, in spirit, similar to the stratified random sampling approach as used in the design of experiments [33].

Assume that we would like to build a library with L pairs of image patches, we randomly sample $K \times L$ HR patches from \mathbf{P}_h 's. Then we apply the k -means method to classify the HR patches into k categories according to the pixel's intensity. After that, we randomly sample L/k HR patches from each category, and store them and their matched upsampled patches \mathbf{P}_r 's in the library. We denote each pair of the patches by $\mathbf{P}_h^{(l)}$ and $\mathbf{P}_r^{(l)}$, for $l = 1, \dots, L$. When we choose a large enough K , say 20, there are usually more than L/k patches in each category. If the number of patches in one category is fewer

Algorithm 1 Registration and paired library building. Inputs: HR image, \mathbf{I}_h , LR image, \mathbf{I}_l , n , k , K , L . Outputs: paired library, $\{\mathbf{P}_h^{(l)}, \mathbf{P}_r^{(l)}\}_{l=1}^L$.

- 1) Enlarge \mathbf{I}_l by 2 times by the bicubic interpretation to obtain an upsampled image. Denote the resulting image by \mathbf{I}_u .
- 2) Search a shifting transform (x, y) and a rotation transformation θ . After the transformation, the overlapping parts on \mathbf{I}_u and \mathbf{I}_h have the smallest mean squared error (MSE). The registered image of \mathbf{I}_u is denoted by \mathbf{I}_r .
- 3) For each $n \times n$ $\mathbf{P}_h(i, j)$, search a local (x_{ij}, y_{ij}) to minimize the MSE between $\mathbf{P}_h(i, j)$ and $\mathbf{P}_r(i+x_{ij}, j+y_{ij})$ from \mathbf{I}_r . The matched patch is denoted by $\mathbf{P}_r(i^*, j^*)$.
- 4) Sample KL patches from \mathbf{P}_h 's, then use k -means method to classify them into k categories.
- 5) Sample L/k patches from each category to obtain a library with L HR patches.
- 6) Add the matched upsampled patch \mathbf{P}_r 's into the library. Each pair is denoted by $\mathbf{P}_h^{(l)}$ and $\mathbf{P}_r^{(l)}$.

then L/k , we can use all the patches in that category. As a result, the library size is then smaller than L , which is fine. In our implementation, we set $K = 20$ and $k = 10$.

In Figure 5, we demonstrate a library with 800 paired 9×9 patches. Figure 5, the right most panel, presents the histogram of patches in the ten categories of the original image data. We can see that the first, fourth and fifth categories account for a large portion of the randomly sampled patches and these categories correspond to the patches in the background area. After the selection, there will be 80 patches in each category equally. Thus background patches only make up 30% of the selected ones in the library, whereas others 70% are the patches with rich texture. Comparing the two figures on the left, we observe that the noise and contrast levels are represented with a good balance in both HR and LR electron image patches.

We summarize the registration step from Section III-A and the paired library building step from Section III-B in Algorithm 1. By default, $n = 9$, $k = 10$, $K = 20$, and L is from a few thousand to tens of thousand.

C. Super-resolution based on Paired LB-NLM

With the paired library, we can reconstruct an HR image for the whole LR image area. The major impact is for the area of the LR image where there is no HR image correspondence. The proposed method is expected to make a positive enhancement.

In doing so, we need to first upsample the input LR image \mathbf{I}_l to \mathbf{I}_u by two times using bicubic interpolation. Then a revised LB-NLM filter, based on the paired library established above, is applied to \mathbf{I}_u to obtain a filtered image \mathbf{I}_f . The filtered image \mathbf{I}_f is the SR reconstruction of the physical LR image \mathbf{I}_l .

Specifically, the algorithm runs as follows. For each pixel (i, j) in \mathbf{I}_u , we extract an $n \times n$ patch $\mathbf{Q}_u(i, j)$ centered at

(i, j) . Then a weight vector, \mathbf{w} , is calculated by comparing \mathbf{Q}_u and the upsampled patches \mathbf{P}_r 's in the paired library as

$$w^{(l)} = \exp \left\{ -\frac{\|\mathbf{Q}_u(i, j) - \mathbf{P}_r^{(l)}\|_2^2}{2n^2\sigma_n^2} \right\}, \quad (2)$$

where σ_n controls the sparsity of the weight vector and can be interpreted as the assumed standard deviation of the image noise [30]. After \mathbf{w} is normalized by $\mathbf{w} / \sum_{l=1}^L w^{(l)}$, the intensity of the filtered image is then calculated as the weighted average of $I_h^{(l)}$, the intensity of the center pixel of the HR patches $\mathbf{P}_h^{(l)}$ in the paired library, such that

$$\mathbf{I}_f(i, j) = \sum_{l=1}^L w^{(l)} I_h^{(l)}. \quad (3)$$

Since the patches in the library have been classified into k categories, we accelerate the LB-NLM filter by only calculating the weights of the category closest to the current patch $\mathbf{Q}_u(i, j)$. As the weights are calculated by an exponential function, their values are close to 0 when a category is dissimilar to the current patch. We compare the average value of the HR patches \mathbf{P}_r 's in each category with $\mathbf{Q}_u(i, j)$ to find the closest category. The selection is based on the shortest Euclidean distance between the average HR patch and $\mathbf{Q}_u(i, j)$. Then the intensity $\mathbf{I}_f(i, j)$ is obtained by the weighted average of the patches in this category alone. This approach can reduce the computational cost by k times.

The scale parameter σ_n can affect the LB-NLM filtering outcomes. For a small σ_n , $\mathbf{I}_f(i, j)$ is determined by a few closest patches, yielding a similar result as the neighborhood embedding method [12]. This line of method helps reconstruct image details in the foreground area. When σ_n is large, LB-NLM averages a large number of patches in the library, decreasing the noise carried over from the training HR images. As EM images usually have a high noise level, especially in the background area, the revised LB-NLM method can provide a good trade-off between enhancing signals and de-noising. We discuss the choice of σ_n more in Section IV.

The key difference between the original LB-NLM in [30] and the proposed method is the way to obtain the weight averages. In [30], both the weight and intensity are calculated from the same HR patches $\mathbf{P}_h^{(l)}$. In our method, the intensity $I_h^{(l)}$ comes still from HR patches $\mathbf{P}_h^{(l)}$ but the weight, $w^{(l)}$, is calculated from $\mathbf{P}_r^{(l)}$. With this change, we establish a direct connection between the physical LR and HR EM images. We outline the steps of the paired LB-NLM in Algorithm 2.

D. Performance Criteria for Nanoimages

To measure the the performance of a SR method, the most popular method is to consider the HR image as the ground truth, and compare it with the reconstructed image by calculating PSNR and SSIM. The closer the two images are, the higher PSNR and SSIM will be. Because bicubic interpolation serves as the baseline method, what is reported in the literature is the delta in PSNR or the delta in SSIM, i.e., the change made by the proposed method over the bicubic interpolation baseline (as seen in the earlier section).

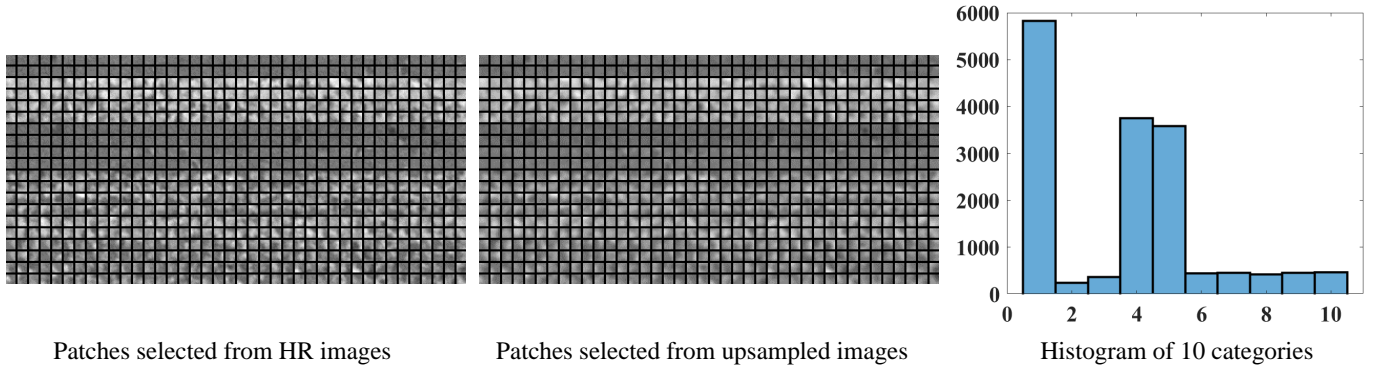


Fig. 5. Demonstration of a paired library with 800 9×9 patches, classified into 10 categories. Left: the selected HR patches, where every rows make up one category; middle: the corresponding upsampled LR patches, right: the histogram of the original patches and the selected patches.

As the foreground and background of EM images vary significantly, we also propose to segment the nanomaterial clusters (foreground) and the host material (background) through image binarization, and evaluate the improvements in PSNR and SSIM separately for the foreground as well as for the background. The foreground improvement reveals how well the SR method enhances the details of the image texture, whereas the background improvement points to a better denoising capability.

As the goal of super-resolution for EM images is to increase the ability of material characterization, like the accuracy of morphology analysis, we propose to add a metric to measure more directly the impact made by the SR method. This measure is to check whether the reconstructed images are able to facilitate a better detection of nanomaterial's boundary.

Algorithm 2 Paired library-based nonlocal-mean filtering. Inputs: n , HR image, \mathbf{I}_h , LR image, \mathbf{I}_l , the paired library, $\{\mathbf{P}_h^{(l)}, \mathbf{P}_r^{(l)}\}_{l=1}^L$; Outputs: SR reconstruction, \mathbf{I}_f .

- 1) Upsample \mathbf{I}_h by the bicubic interpolation by 2 times to \mathbf{I}_u .
- 2) Obtain an $n \times n$ patch $\mathbf{Q}_u(i, j)$ from \mathbf{I}_u .
- 3) We denote the weight vector by $\mathbf{w} = \{w^{(1)}, w^{(2)}, \dots, w^{(L)}\}$. For $l = 1, 2, \dots, L$, the weight $w^{(l)}$ is calculated as:

$$w^{(l)} = \exp \left\{ -\frac{\|\mathbf{Q}_u(i, j) - \mathbf{P}_r^{(l)}\|_2^2}{2n^2\sigma_n^2} \right\},$$

where σ_n^2 is the scale parameter of the LB-NLM filter.

- 4) Normalize \mathbf{w} by

$$w^{(l)} = \frac{w^{(l)}}{\sum_{l=1}^L w^{(l)}}.$$

- 5) $\mathbf{I}_f(i, j)$ is the weighted average of $\mathbf{I}_h^{(l)}$ as:

$$\mathbf{I}_f(i, j) = \sum_{l=1}^L w^{(l)} \mathbf{I}_h^{(l)},$$

where $\mathbf{I}_f(i, j)$ is the intensity of the center pixel of $\mathbf{P}_h^{(l)}$.

For that, we use the Canny edge detector [34] to identify the boundaries and textures of the nanomaterial clusters and label the detected edges in a binary map. Let B_{HR} denote the binary edge map detected from the original HR image (ground truth) and B_{SR} denote the binary map detected from the reconstructed image resulting from the proposed SR method. The similarity between them is defined as:

$$\text{sim} = 1 - \frac{\|B_{\text{HR}} \neq B_{\text{SR}}\|_1}{\|B_{\text{HR}}\|_1 + \|B_{\text{SR}}\|_1}, \quad (4)$$

where $\|\cdot\|_1$ is the summation of all the elements of the binary map. A high sim indicates a better performance.

IV. EXPERIMENTAL RESULTS

A. SEM Images

To test the proposed SR method, we collect 22 pairs of SEM images with low and high resolutions. The resolution of HR images double that of the LR ones, so that the scale ratio is 2:1. The size of both types of images is $1,280 \times 944$ pixels. Through image registration, we identify the overlapping areas of each pair and carve out the corresponding LR image, which is of 640×472 pixels. The $1,280 \times 944$ -pixel HR image and the 640×472 -pixel LR image are what we used to train the model and do the testing. The non-overlapping area of the LR image is not used in the experimental analysis.

To have a fair test which could mimic the practical applications where the SR method is to be applied to the area where there is no corresponding HR images, we partition the LR image and HR image in each pair into 3×4 subimages. We then build the library using nine out of the 12 subimages and keep the remaining three subimages unused in the learning stage and treat them as the out-of-sample test data. The size of an HR subimage is 320×314 , where the size of an LR subimage is 160×157 , still maintaining the 2:1 ratio, as dictated by their resolution difference. The training and test subimages of two SEM image pairs are shown in Figure 6.

B. Determining the Training Strategy

Before we implement the SR method, we would like to discuss briefly the training strategy. To reconstruct the test

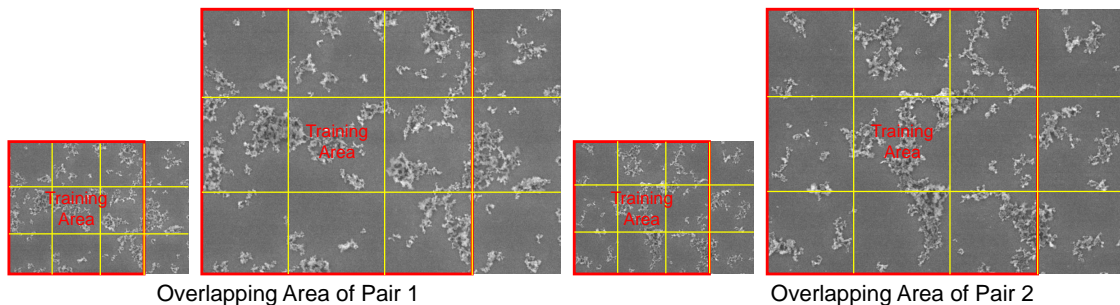


Fig. 6. The overlapping areas of two pairs of SEM images. The left 75% is the training area and the right 25% is the test area. The yellow lines partition each image into 3×4 subimages.

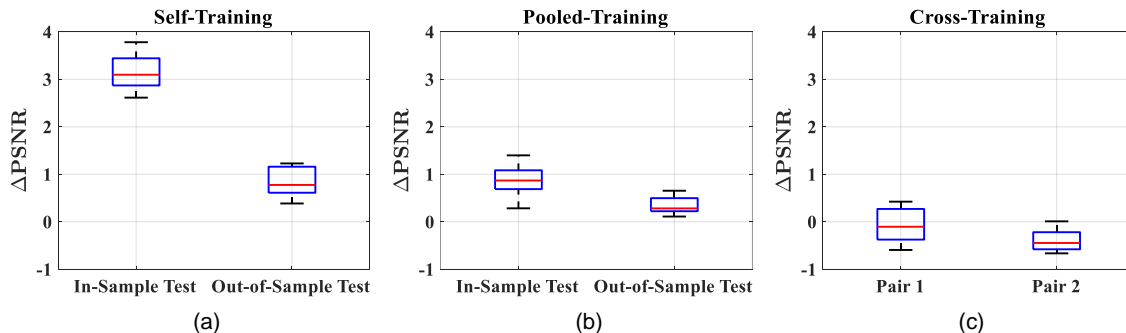


Fig. 7. The change in PSNR when the reconstructed EM images by the paired LB-NLM method as compared with those by bicubic interpolation. The three plots are the results obtained with the three training strategies.

subimages from Pair 1, we can use its own training area (the 9 subimages on the left) to train a library, or alternatively, combine the training areas of Pair 1 and Pair 2 together. We refer to the former as self-training and the latter as pooled-training. We can also reconstruct the testing images from Pair 1 using the library sampled from Pair 2, which is referred to as cross-training.

We test the three training strategies on two pairs of images shown in Figure 6 using the proposed SR method, and record the change in PSNR as compared with bicubic interpolation; the results are in Figure 7. For self-training and pooled-training, the in-sample results are based on 18 subimages in the training areas, whereas the out-of-sample results use the remaining 6 subimages outside the training area. For cross-training, as the library is trained from the other pair, all the results are out-of-sample.

In most of SR works on optical images, the popular strategy is the pooled training, as a large sample size usually yields a better model. But Figure 7 shows that the performance of self-training is apparently better than the other two strategies when it comes to these EM images (similar experimental results can be obtained from other pairs of EM images as well). We believe this is something unique for the paired physical image problem—when a physical LR image is involved, using the paired library sampled from the pair’s own overlapping area can lead to a better reconstruction results, as the training data involving the pair embody information directly relevant to the difference between the two images. We try as well the

three training strategies on our EM image pairs but using the VDSR method. The self-training still outperforms the other two strategies; the numerical results are omitted here.

C. General Results of PSNR and SSIM

With self-training, we test the proposed method on the 22 pairs of SEM images, partitioned into 198 in-sample subimages and 66 out-of-sample subimages. A library with $L = 80,000$ 9×9 paired patches is sampled by using Algorithm 1 for a pair of images. The paired LB-NLM algorithm as in Algorithm 2 reconstructs the HR images from the LR subimages. For the purpose of comparison, we implement the original LB-NLM filter [30], the sparse-representation based SR [21], and VDSR [25] and apply them to our EM images.

For both the original and paired LB-NLM, we need to decide the tuning parameter σ_n in equation (2) while calculating the weight vector \mathbf{w} . There are two ways to interpret σ_n . For image de-noising, σ_n indicates the assumed standard deviation of the image noise. The noisier the input images are, the larger σ_n we need to choose. The value of σ_n also controls the sparsity of the weigh vector \mathbf{w} . When σ_n is small, only a few $w^{(l)}$ ’s, which correspond to the closest patches in the library, are non-zero. In our experiments, we explore $\sigma_n = 0.1, 1.0, 2.0$ for both the original and the paired LB-NLM methods. What we do is that we first use $\sigma_n = 1.0$ as the default setting and later present a sensitivity analysis.

Table I presents the average improvement of PSNR and SSIM by different SR methods as compared with bicubic

interpolation. The sparse-representation SR method and VDSR perform similarly to bicubic interpolation but slightly worse—both methods yield negative changes in PSNR and SSIM. The original LB-NLM method can increase PSNR and SSIM. Interestingly, the amount of improvement made by the original LB-NLM are similar for the in-sample cases versus the out-of-sample case. While it may sound counterintuitive, it is not surprising, as the LB-NLM does not use the LR physical images in its training but only the HR patches, so that HR and LR images are not really paired together. As a result, there is not much difference between in-sample tests and out-of-sample tests.

The proposed paired LB-NLM achieves the most significant improvement in both PSNR and SSIM. For the in-sample subimages, it increases, on average, PSNR by 3.75 dB and SSIM by 0.132, whereas for the out-of-sample subimages, its average improvement is 1.66 dB in terms of PSNR and 0.036 in terms of SSIM. The performance on the out-of-sample tests is, as expected, not as good as the in-sample results—the difference of the in-sample versus out-of-sample tests also highlights the use of the paired image patches in the proposed method. The paired LB-NLM, even in terms of the out-of-sample test performance, still outperforms other methods by a large margin. When we apply the proposed method to the non-overlapping area of the LR image, we expect to achieve similar performance as the out-of-sample results.

Let us take a closer look at the reconstruction results. To get an intuitive feeling, we present in Figures 8 and 9 the original LR images, bicubic interpolated images, the reconstructed images by the original LB-NLM method, the reconstructed images by the paired LB-NLM method, and the HR images (ground truth). In each figure, four images are shown. The four images in Figure 8 are in-sample subimages, whereas those in Figure 9 are out-of-sample subimages. As the sparse-representation based method and the VDSR produce very similar results as bicubic interpolation, we skip the presentation of their results in this visual comparison.

In Figure 8, it is clear to see that the paired LB-NLM method achieves the best SR performance. While the original LB-NLM is able to improve PSNR and SSIM, the results are blurred as compared with the bicubic interpolated images. The proposed paired LB-NLM method gives us a clear foreground area and a much less noisy background one. For the third in-sample subimage, the paired LB-NLM method obtains a nearly 10 dB improvement as compared with bicubic interpolation, while the original LB-NLM can improve by roughly 2 dB. We believe that the reason behind this large improvement for this particular image is because the contrasts of the LR and HR images are significantly different. The background of the LR image is darker than that of the HR image. Thanks to the paired LR and HR patches in the library, the paired LB-NLM method can adjust the image contrast automatically when reconstructing the image, making the reconstruction results better quality.

For the out-of-sample subimages in Figure 9, we have a similar observation. The proposed method still consistently outperforms the original LB-NLM. For the first, second and fourth image, the improvement in PSNR is about 1 ~ 2

dB, while for the third image, the improvement is more than 6 dB. Admittedly but not surprisingly, the out-of-sample reconstruction results are not as good as those in-sample ones.

Next, we conduct a sensitivity analysis on σ_n using the original and paired LB-NLM methods. Three values of σ_n are used: 0.1, 1.0 and 2.0. Table II presents the analysis results.

For the original LB-NLM, its performance becomes better when we choose a large σ_n , although the difference is not much. Its best improvement is appreciably weaker than the out-of-sample performance of the paired LB-NLM. For the proposed paired LB-NLM, the trends for the in-sample and out-of-sample images are different. In the former case, a small σ_n is preferred as this setting can enhance the fine texture in the foreground. In the latter case a large σ_n produces a slightly better results as that setting suppresses the background more while also blurring the foreground signals. When we analyze the performance in the background and foreground separately, we find that the moderate value of σ_n , say 1.0, provides a good trade-off and we thus recommend this value as the default.

D. Further Performance Analysis

In this section, we provide quantitative analysis using the new criteria for EM nanoimages: the separate foreground and background analysis and the edge detection analysis.

We first segment the SEM images by using Otsu's method [35] to highlight the separation of foreground from background and remove the isolated noise points in the foreground. Figure 10 shows the binary masks indicating the foreground versus the background in two images. Then we calculate separately the improvements of PSNR made by the proposed method in the foreground and background. As the previous studies show that the change in SSIM is consistent with that in PSNR, we skip the calculation of SSIM here.

Table IV presents the changes in PSNR calculated for foreground and background under different σ_n settings. For the in-sample subimages, we observe that the paired LB-NLM method improves both foreground and background but the improvement in foreground slightly outweigh that in background. Also, a large σ_n has a detrimental effect on both foreground and background.

For the out-of-sample subimages, the paired LB-NLM method improves the quality of background much greater than that of foreground. It appears to us that the merit of the proposed paired LB-NLM method is to suppress the background noise, without degrading the quality of the foreground signals, so that the foreground signals stand out more. When we change σ_n , the foreground quality benefits from a small σ_n value, as it sharpens the fine texture, while the background quality benefit from a large σ_n value, as it suppresses the background noise more (but also blurs the fine texture). The middle value of $\sigma_n = 1.0$ seems to be a good trade-off.

Next, we apply the Canny edge detector [34] to the HR images, the bicubic interpolated images, and the reconstruction images by the proposed method, with a key Canny edge detector's parameter set as 0.2. Figure 11 demonstrates the detection results for both an in-sample and out-of-sample subimage. The visual inspection shows clearly that our reconstruction results facilitate more accurate edge detections than

TABLE I
THE IMPROVEMENTS OF PSNR AND SSIM OF THE RECONSTRUCTED SEM IMAGES AFTER APPLYING DIFFERENT SR METHODS, AS COMPARED WITH BICUBIC INTERPOLATION.

		Original LB-NLM [30]	Proposed Paired LB-NLM	Sparse Method [21]	VDSR [25]
In-Sample	Δ PSNR	0.46 dB	3.75 dB	-0.07 dB	-0.10 dB
	Δ SSIM	0.016	0.132	-0.008	-0.010
Out-of-Sample	Δ PSNR	0.45 dB	1.66 dB	-0.08 dB	-0.10 dB
	Δ SSIM	0.015	0.036	-0.009	-0.010

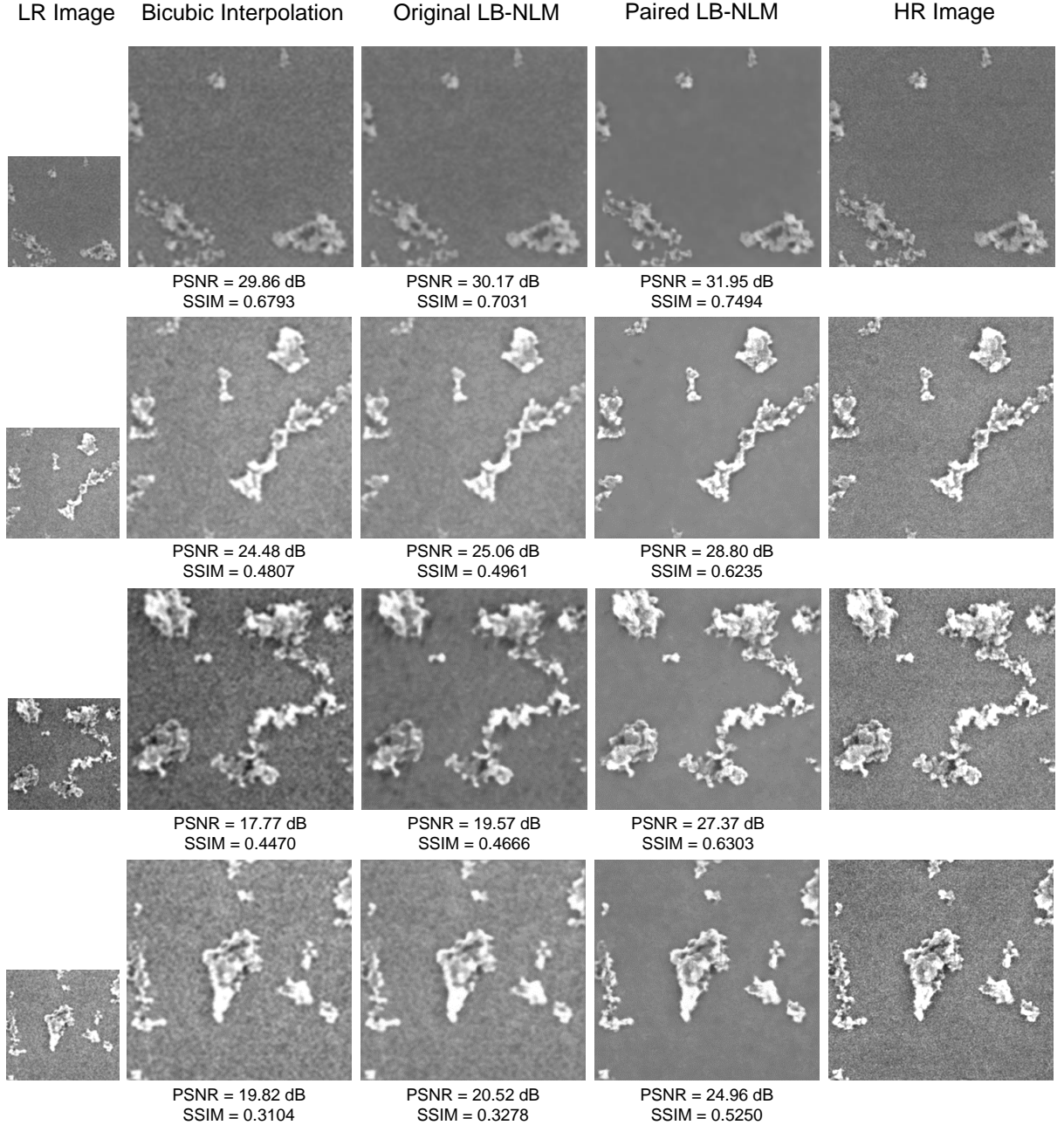


Fig. 8. The LR images, the bicubic interpolated results, the image reconstruction results by using the original and paired LB-NLM methods, and the ground truth (HR images) for four in-sample subimages ($\sigma_n = 1.0$).

the bicubic interpolated images when both are compared with the boundaries detected in the HR images (the ground truth).

To quantify the improvement in edge detection accuracy, we

calculate the similarity index, sim, as defined in equation (4) in Section III-D. For the paired LB-NLM methods, we again try different values of σ_n . Compared with bicubic interpolation,

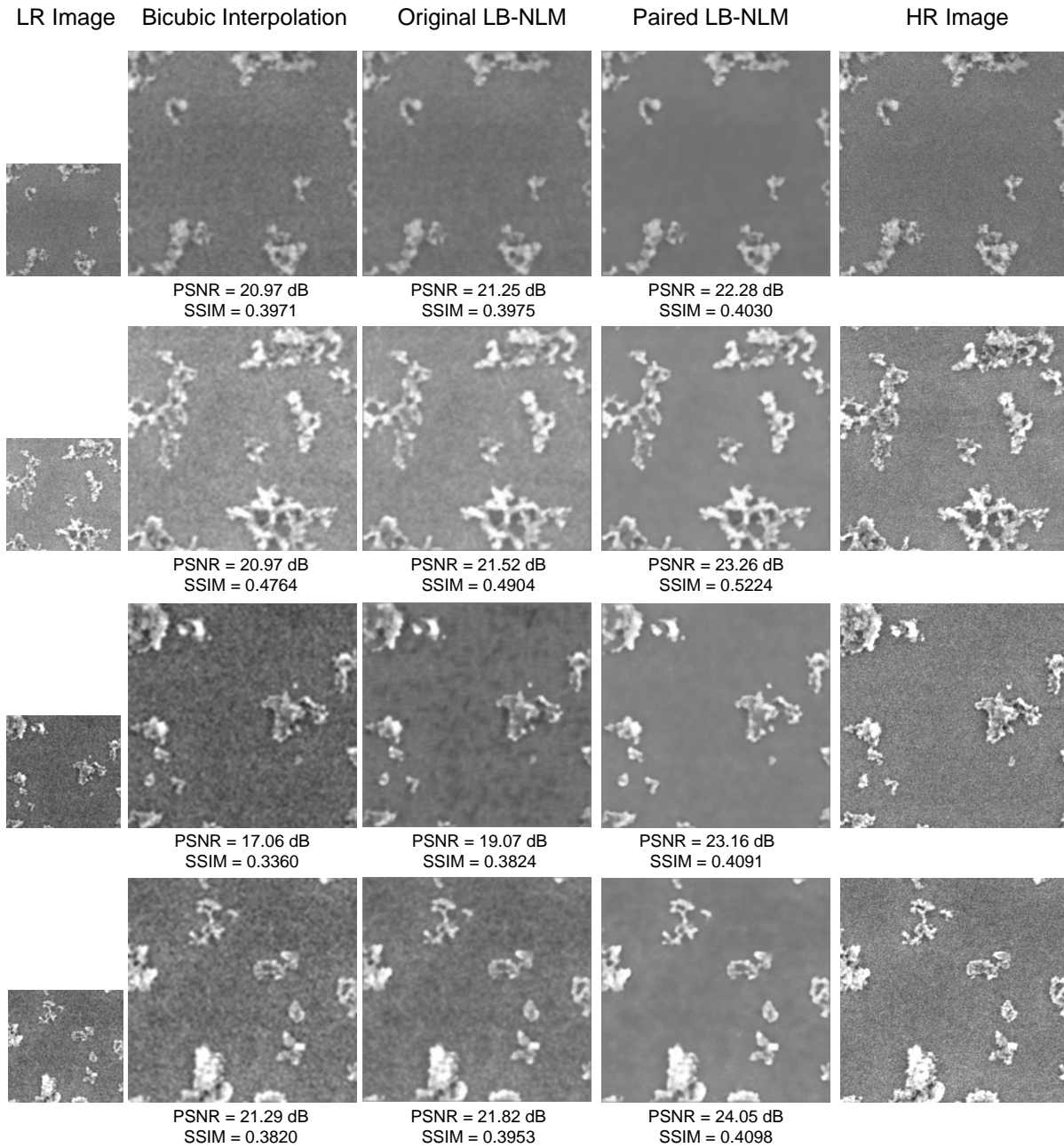


Fig. 9. The LR images, the bicubic interpolated results, the image reconstruction results by using the original and paired LB-NLM methods, and the ground truth (HR images) for four out-of-sample subimages ($\sigma_n = 1.0$).

TABLE II
THE IMPROVEMENTS OF PSNR AND SSIM OF THE RECONSTRUCTED SEM IMAGES BY THE PAIRED AND ORIGINAL LB-NLM METHODS WITH DIFFERENT σ_n 'S.

σ_n		0.1	1.0	2.0
Original LB-NLM [30]				
In-Sample	Δ PSNR	0.45 dB	0.46 dB	0.60 dB
	Δ SSIM	0.015	0.016	0.022
Out-of-Sample	Δ PSNR	0.45 dB	0.45 dB	0.60 dB
	Δ SSIM	0.015	0.015	0.022
Paired LB-NLM (proposed method)				
In-Sample	Δ PSNR	3.87 dB	3.75 dB	3.35 dB
	Δ SSIM	0.145	0.132	0.089
Out-of-Sample	Δ PSNR	1.64 dB	1.64 dB	1.87 dB
	Δ SSIM	0.034	0.036	0.038

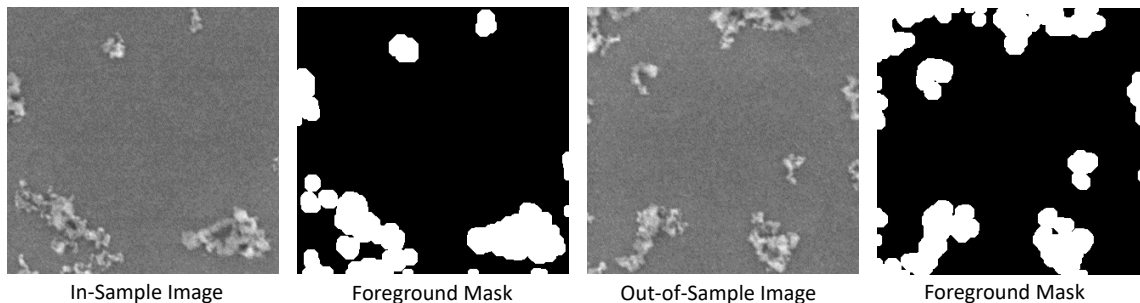


Fig. 10. The foreground and background masks of an in-sample and an out-of-sample SEM subimage. The white areas indicate the nanomaterial (foreground), whereas the black areas indicate the host material (background).

TABLE III
CHANGES IN PSNR CALCULATED FOR FOREGROUND AND BACKGROUND UNDER DIFFERENT σ_n SETTINGS.

σ_n		0.1	1.0	2.0
In-Sample	Foreground	4.28 dB	4.27 dB	4.06 dB
	Background	3.68 dB	3.52 dB	3.04 dB
Out-of-Sample	Foreground	0.23 dB	0.23 dB	0.22 dB
	Background	2.61 dB	2.65 dB	2.67 dB

the proposed method improves the sim metric by the amount of 0.31, or a relative improvement of 130%, for the in-sample images, and by the amount of 0.09, or a relative improvement of 38%, for the out-of-sample images. We also observe that the performance of the proposed method remains reasonably robust under varying σ_n . Nonetheless, a too large σ_n is still to be avoided because the performance of edge detection suffers considerably from image blurring, which tends to take place under a large σ_n .

V. CONCLUSIONS AND FUTURE WORK

Our research identifies new issues and challenges in super-resolution research that have not received enough attention. Specifically, we propose a super-resolution method to enhance a physical LR electron image based on the LR/HR electron image pairs. The main contributions of our research are summarized below:

- We propose a global and local registration algorithm to identify the overlapping area and individual matched patches between the HR and LR electron images.
- We improve the original LB-NLM method by introducing a paired library to connect the HR and LR patches, and develop a clustering approach to select the representative patches into the paired library.
- We test our method using existing as well as newly introduced performance criteria and demonstrate how the proposed method works and where it makes greater impacts.

Our effort is among the very early efforts in addressing the new issues and we are delighted that as compared with the existing SR approaches, this initial effort makes appreciable improvement on the problem at hand. By introducing the new SR problem, we hope that much more is to come and are confident that more competent methods will be developed in due course. Some immediate needs for improvement come

to mind, including (a) how to further enhance the quality of foreground while maintaining the gain in background quality for out-of-sample images, and (b) whether we can construct a unified framework for handling the registration/distortion problem in paired electron images, rather than using a multi-step sequential procedure as proposed here.

ACKNOWLEDGMENT

The authors would like to acknowledge the generous support from their sponsors. This work is partially supported by AFOSR DDDAS program grants FA9550-18-1-0144 and Texas A&M X-grant program.

REFERENCES

- [1] C. Park, J. Huang, D. Huitink, S. Kundu, B. Mallick, H. Liang, and Y. Ding, "A multi-stage, semi-automated procedure for analyzing the morphology of nanoparticles," *IIE Transactions Special Issue on Nanomanufacturing*, vol. 44, no. 7, pp. 507–522, 2012.
- [2] C. Park, J. Huang, J. Ji, and Y. Ding, "Segmentation, inference and classification of partially overlapping nanoparticles," *IEEE Transactions on Pattern Analysis and Machine Intelligence*, vol. 35, no. 3, pp. 669–681, 2013.
- [3] H. Yang and N. Ahuja, "Automatic segmentation of granular objects in images: Combining local density clustering and gradient-barrier watershed," *Pattern Recognition*, vol. 47, no. 6, pp. 2266–2279, 2014.
- [4] Y. Qian, J. Z. Huang, X. Li, and Y. Ding, "Robust nanoparticles detection from noisy background by fusing complementary image information," *IEEE Transactions on Image Processing*, vol. 25, no. 12, pp. 5713–5726, 2016.
- [5] S. C. Park, M. K. Park, and M. G. Kang, "Super-resolution image reconstruction: A technical overview," *IEEE Signal Processing Magazine*, vol. 20, no. 3, pp. 21–36, 2003.
- [6] J. Tian and K.-K. Ma, "A survey on super-resolution imaging," *Signal, Image and Video Processing*, vol. 5, no. 3, pp. 329–342, 2011.
- [7] L. Yue, H. Shen, J. Li, Q. Yuan, H. Zhang, and L. Zhang, "Image super-resolution: The techniques, applications, and future," *Signal Processing*, vol. 128, no. 11, pp. 389–408, 2016.

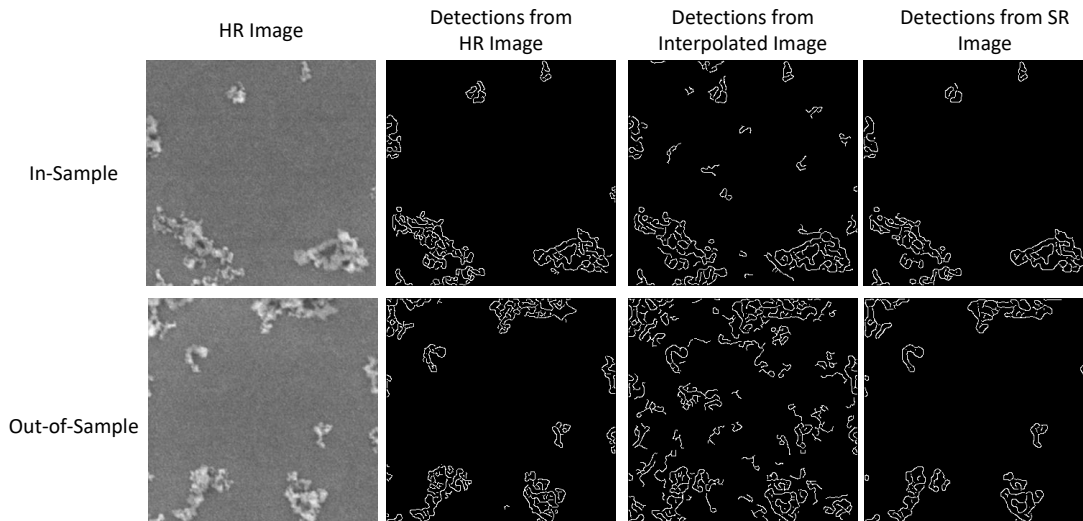


Fig. 11. The results of the Canny edge detection from the HR images and the reconstruction images by using bicubic interpolation and the proposed SR method, respectively.

TABLE IV
RESULTS OF SIM FOR THE PROPOSED METHOD UNDER DIFFERENT σ_n 'S AND BICUBIC INTERPOLATION.

Method	Bicubic Interpolation	Paired LB-NLM		
		$\sigma_n = 0.1$	$\sigma_n = 0.5$	$\sigma_n = 1.0$
In-Sample	0.25	0.58	0.58	0.56
Out-of-Sample	0.24	0.33	0.33	0.33

- [8] R. Timofte, E. Agustsson, L. Van Gool, M.-H. Yang, and L. Zhang, "NTIRE 2017 challenge on single image super-resolution: Methods and results," *Proceedings of the IEEE Conference on Computer Vision and Pattern Recognition Workshops (CVPRW)*, pp. 114–125, 2017.
- [9] T. Komatsu, T. Igarashi, K. Aizawa, and T. Saito, "Very high resolution imaging scheme with multiple different-aperture cameras," *Signal Processing: Image Communication*, vol. 5, no. 5-6, pp. 511–526, 1993.
- [10] N. R. Shah and A. Zakhori, "Resolution enhancement of color video sequences," *IEEE Transactions on Image Processing*, vol. 8, no. 6, pp. 879–885, 1999.
- [11] W. T. Freeman, T. R. Jones, and E. C. Pasztor, "Example-based super-resolution," *IEEE Computer Graphics and Applications*, vol. 22, no. 2, pp. 56–65, 2002.
- [12] H. Chang, D.-Y. Yeung, and Y. Xiong, "Super-resolution through neighbor embedding," *Proceedings of the IEEE Conference on Computer Vision and Pattern Recognition (CVPR)*, pp. 1–8, 2004.
- [13] T.-M. Chan, J. Zhang, J. Pu, and H. Huang, "Neighbor embedding based super-resolution algorithm through edge detection and feature selection," *Pattern Recognition Letters*, vol. 30, no. 5, pp. 494–502, 2009.
- [14] X. Gao, K. Zhang, D. Tao, and X. Li, "Image super-resolution with sparse neighbor embedding," *IEEE Transactions on Image Processing*, vol. 21, no. 7, pp. 3194–3205, 2012.
- [15] P. Sandeep and T. Jacob, "Single image super-resolution using a joint GMM method," *IEEE Transactions on Image Processing*, vol. 25, no. 9, pp. 4233–4244, 2016.
- [16] Y. Huang, J. Li, X. Gao, L. He, and W. Lu, "Single image super-resolution via multiple mixture prior models," *IEEE Transactions on Image Processing*, vol. 27, no. 12, pp. 5904–5917, 2018.
- [17] K. S. Ni and T. Q. Nguyen, "Image superresolution using support vector regression," *IEEE Transactions on Image Processing*, vol. 16, no. 6, pp. 1596–1610, 2007.
- [18] K. I. Kim and Y. Kwon, "Single-image super-resolution using sparse regression and natural image prior," *IEEE Transactions on Pattern Analysis and Machine Intelligence*, vol. 32, no. 6, pp. 1127–1133, 2010.
- [19] R. Timofte, V. De Smet, and L. Van Gool, "A+: Adjusted anchored neighborhood regression for fast super-resolution," *Proceedings of the Asian Conference on Computer Vision (ACCV)*, pp. 111–126, 2014.
- [20] H. Wang, X. Gao, K. Zhang, and J. Li, "Single-image super-resolution using active-sampling gaussian process regression," *IEEE Transactions on Image Processing*, vol. 25, no. 2, pp. 935–948, 2016.
- [21] J. Yang, J. Wright, T. S. Huang, and Y. Ma, "Image super-resolution via sparse representation," *IEEE Transactions on Image Processing*, vol. 19, no. 11, pp. 2861–2873, 2010.
- [22] J. Yang, Z. Wang, Z. Lin, S. Cohen, and T. Huang, "Coupled dictionary training for image super-resolution," *IEEE Transactions on Image Processing*, vol. 21, no. 8, pp. 3467–3478, 2012.
- [23] S. Wang, L. Zhang, Y. Liang, and Q. Pan, "Semi-coupled dictionary learning with applications to image super-resolution and photo-sketch synthesis," *Proceedings of the IEEE Conference on Computer Vision and Pattern Recognition (CVPR)*, pp. 2216–2223, 2012.
- [24] C. Dong, C. C. Loy, K. He, and X. Tang, "Learning a deep convolutional network for image super-resolution," *Proceedings of the European Conference on Computer Vision (ECCV)*, pp. 184–199, 2014.
- [25] J. Kim, J. Kwon Lee, and K. Mu Lee, "Accurate image super-resolution using very deep convolutional networks," *Proceedings of the IEEE Conference on Computer Vision and Pattern Recognition (CVPR)*, pp. 1646–1654, 2016.
- [26] B. Lim, S. Son, H. Kim, S. Nah, and K. Mu Lee, "Enhanced

- deep residual networks for single image super-resolution,” *Proceedings of the IEEE Conference on Computer Vision and Pattern Recognition Workshops (CVPRW)*, pp. 136–144, 2017.
- [27] Z. Wang, A. C. Bovik, H. R. Sheikh, and E. P. Simoncelli, “Image quality assessment: From error visibility to structural similarity,” *IEEE Transactions on Image Processing*, vol. 13, no. 4, pp. 600–612, 2004.
- [28] M. Grubinger, P. Clough, H. Müller, and T. Deselaers, “The IAPR TC-12 benchmark: A new evaluation resource for visual information systems,” *Proceedings of the OntoImage Workshop on Language Resources for Content-based Image Retrieval*, pp. 13–22, 2006.
- [29] R. Keys, “Cubic convolution interpolation for digital image processing,” *IEEE Transactions on Acoustics, Speech, and Signal Processing*, vol. 29, no. 6, pp. 1153–1160, 1981.
- [30] S. Sreehari, S. Venkatakrisnan, K. L. Bouman, J. P. Simmons, L. F. Drummy, and C. A. Bouman, “Multi-resolution data fusion for super-resolution electron microscopy,” *Proceedings of the IEEE Conference on Computer Vision and Pattern Recognition Workshops (CVPRW)*, pp. 1084–1092, 2017.
- [31] S. Boyd, N. Parikh, E. Chu, B. Peleato, and J. Eckstein, “Distributed optimization and statistical learning via the alternating direction method of multipliers,” *Foundations and Trends in Machine Learning*, vol. 3, no. 1, pp. 1–122, 2011.
- [32] X. Zhang, Q. Chen, R. Ng, and V. Koltun, “Zoom to learn, learn to zoom,” *Proceedings of the IEEE Conference on Computer Vision and Pattern Recognition (CVPR)*, pp. 1–8, 2019.
- [33] D. C. Montgomery, *Design and Analysis of Experiments*. John Wiley & Sons, 2017.
- [34] C. G. Harris and M. Stephens, “A combined corner and edge detector,” *Alvey Vision Conference*, vol. 15, no. 50, pp. 10–5244, 1988.
- [35] N. Otsu, “A threshold selection method from gray-level histograms,” *IEEE Transactions on Systems, Man, and Cybernetics*, vol. 9, no. 1, pp. 62–66, 1979.